LASER SPECTROSCOPY SENSORS FOR MEASUREMENT OF TRACE GASEOUS FORMALDEHYDE

by

Ravi Kumar. Boddeti

Submitted in Partial Fulfillment of the Requirements

for the Degree of

Masters of Science

in the

Chemistry

Program

YOUNGSTOWN STATE UNIVERSITY
August 2008

LASER SPECTROSCOPY SENSORS FOR MEASUREMENT OF TRACE GASEOUS FORMALDEHYDE

Ravi Kumar. Boddeti

I hereby release this thesis to the public. I understand that this thesis will be made available from the OhioLINK ETD Center and the Maag Library Circulation Desk for public access. I also authorize the University or other individuals to make copies of this thesis as needed for scholarly research.

Signature:

_____

Ravi Kumar. Boddeti, Student Date

Approvals:

_____

Joseph B. Simeonsson, Ph.D., Thesis Advisor Date

_____

Michael A. Serra, Ph. D., Committee Member Date

_____

Larry S. Curtin, Ph. D., Committee Member Date

_____

Peter J. Kasvinsky, Dean of School of Graduate Studies & Research Date

Abstract: A sensitive and direct method to determine atmospheric formaldehyde (HCHO) using laser induced fluorescence spectroscopy (LIF) is described. This technique overcomes the tedious sample collections, water extraction and chemical reactions that are often required in conventional methods. In this LIF approach, the third harmonic of a nontunable Nd:YAG laser at 355 nm is used as a selective excitation wavelength for formaldehyde. Studies at alternative excitation wavelengths have also been performed using 341 nm and 309 nm, which are obtained by Stimulated Raman Scattering of nontunable Nd:YAG laser radiation at 266 nm and 355 nm, respectively. The calibration response is linear in the range of 1-57 ppm and the current limit of detection (LOD) is 0.5 ppm HCHO. It is anticipated that these approaches may be able to avoid interferences that occur in conventional methods for HCHO measurements.

ACKNOWLEDGEMENTS

I acknowledge my sincere thanks to my family members, who supported me for doing Masters. I extend my sincere thanks to my research advisor, Dr. J.B. Simeonsson for all his support and encouragement. I am grateful for the support from my friends at times when I was low. I extend my thanks to my thesis committee members, Dr. Serra and Dr. Curtin for their efforts to see me through graduation.

TABLE OF CONTENTS

LIST OF FIGURES

LIST OF TABLES

LIST OF SYMBOLS AND ABBREVIATIONS

µg	Microgram
m	Meter
m^3	Cubic meter
LIF	Laser Induced Fluorescence
CO	Carbon monoxide
HCHO	Formaldehyde
SRS	Stimulated Raman Scattering
ν	Frequency
Nd: YAG	Neodymium yttrium aluminum garnet
CDC	Centers for Disease Control
FEMA	Federal Emergency Management Agency
ppm	Parts per million
ppb	Parts per billion
GC	Gas chromatography
HPLC	High performance liquid chromatography
DNPH	2,4- dinitrophenylhydrazine
UV-VIS	Ultraviolet-visible
LIDAR	Light detection and ranging
PAH	Polycyclic aromatic hydrocarbons
cm	Centimeter
LP	Long pass

BP	Band pass
ND	Neutral density
SP	Short pass
LOD	Limit of detection
LOQ	Limit of quantification
ng	Nanogram
THG	Third Harmonic generator
FHG	Fourth Harmonic generator
PMT	Photomultiplier tube
GI	Gated integrator
FL	Focusing lens
P	Prisms
nm	nanometer
mV	millivolt
mJ	milliJoule
V	Volt
µ	Micron
µm	Micrometer

1.0 Introduction:

Formaldehyde is the most abundant gas-phase carbonyl compound in the atmosphere. It is found in urban air, at remote locations in the troposphere, [30] and in rain water. [31] The concentration of formaldehyde (HCHO) ranges from tenths of μg m^{-3} in relatively clean air to hundreds of μg m^{-3} in polluted air, and is produced by combustion sources and the photo-oxidation of hydrocarbons.[3] It is also formed as an intermediate in the oxidation of many biogenic and anthropogenic volatile organic compounds. The main reaction pathway for HCHO degradation in the atmosphere is photolysis by ultraviolet radiation. There are two major photolysis pathways. The first produces radicals (equation 1) and the second produces CO and H_2 (equation 4). [14]

$$CH_2O + h\nu \rightarrow HCO^{\cdot} + H \quad (1)$$

$$HCO^{\cdot} + O_2 \rightarrow CO + HO_2^{\cdot} \quad (2)$$

$$H^{\cdot} + O_2 + M \rightarrow HO_2^{\cdot} + M \quad (3)$$

$$CH_2O + h\nu \rightarrow CO + H_2 \quad (4)$$

The photolysis of HCHO can produce radicals as shown in equation (1). The formyl radical and hydrogen atom produced in equation (1) can react with molecular oxygen to form hydroperoxyl radicals as shown in equations (2&3).[14] These radicals can then react with nitrogen oxides to form atmospheric ozone.[1] By either of the two pathways, a photolysis product of HCHO is carbon monoxide that acts as a major sink for atmospheric OH.[2] As a result, formaldehyde is an important compound in understanding the oxidizing ability of the atmosphere and the formation of atmospheric ozone.[26,27]

Formaldehyde is also associated with the 'cool flame' phenomenon, which appears when many hydrocarbon fuel and air mixtures approach the explosion limit.[3] Excited formaldehyde is responsible for the blue chemiluminescence that can be seen in a cool burning flame. As a result, formaldehyde is an indicator of cool flame regions and can be used to study the initiation and progression of combustion.[3]

Formaldehyde has many industrial uses. It is often used for the production of polymers and other chemicals. When it is reacted with phenol, urea, or melamine it produces phenol formaldehyde resin, urea formaldehyde resin, and melamine resin, respectively. These resins are commonly used in permanent adhesives, including those used in plywood or carpeting. Formaldehyde is also used as an embalming agent, and as a preservative in some paints, coatings and cosmetics.[1]

The purpose of the current research project is to investigate a direct approach for measuring formaldehyde in air by fluorescence spectroscopy using a nontunable Nd:YAG laser source. The long term goal of this project is to develop a simple, sensitive, and direct LIF sensor approach that uses fiber optics for rapid and convenient monitoring of formaldehyde in the environment. It is anticipated that this sensor approach will have advantages over conventional methods used for formaldehyde monitoring.

1.1 Sources:

Formaldehyde (HCHO) is formed in the atmosphere through the oxidation of hydrocarbons. For example, formaldehyde can be formed in the reaction of ozone with 1-alkenes (5).[14]

$$RCH=CH_2 + O_3 \rightarrow RCHOO + CH_2O \qquad (5)$$

The most significant sources of formaldehyde in indoor environments are likely to be pressed wood products made using adhesives that contain urea-formaldehyde resins. Fuel-burning appliances, carpets and paneling, glues, textiles, and tobacco smoke are other indoor sources of formaldehyde.[4,28] It is also emitted directly from disinfectants, fungicides, germicides, cosmetics and preservative agents.[14,29,30] In particle board and other wood boards, the materials can be bonded by UF (urea-formaldehyde) resin which in latent form has unstable chemical groups that undergo hydrolysis and can release formaldehyde.[5] Anthropogenic sources of formaldehyde include vehicular and industrial emissions. The industrial sources for formaldehyde are manufacture of non-metallic mineral products, followed by production of fabricated metal products.

A recent example of formaldehyde exposure was by persons living in newly constructed trailers used as temporary housing following hurricane Katrina. These trailers were given to the evacuees from the hurricane. The officials from the Centers of Disease Control (CDC) tested the persons who stayed in the trailers for more than eighteen months and the results indicated that formaldehyde levels were about 500 percent higher than normal. According to FEMA (Federal Emergency Management Agency), the levels of formaldehyde in normal U.S homes are around 10- 50 ppb, whereas in the case of these trailers the levels of formaldehyde were approximately 100 ppb.

As a pollutant, formaldehyde has significant toxicological effects. It causes watery eyes, burning sensations in the eyes and throat, nausea, wheezing, skin rashes, allergic reactions and difficulty in breathing in some humans exposed at levels above 0.1 ppm. In

industrial settings, exposure to formaldehyde has been associated with cancer of nasal cavities, nasopharynx, prostate, lungs, and pancreas. Animals exposed to formaldehyde are more prone to nasal cancer. Because of its toxicity and possible carcinogenic properties, the occupational safety and health organizations of many countries have established an 8 hour time-average permissible exposure limit for formaldehyde ranging from 0.5 ppm to 2.0 ppm.[31]

1.2 STATE OF THE ART FOR HCHO MEASUREMENTS:

Several methods for formaldehyde measurement have been reported. Most of the measurement methods rely on spectrophotometry or chromatography, either gas-chromatography (GC) or high performance liquid chromatography (HPLC), and colorimetry.[6] Colorimetry is commonly used as a reference method for formaldehyde measurements. The chromotropic acid method and pararosaniline method are popular for detection of formaldehyde. The chromotropic acid method is based on the reaction of the formaldehyde-bisulfite adduct with chromotropic acid in the presence of sulfuric acid. A highly colored product is formed that is measured by its absorbance at 580 nm.[6] As the colorimetry methods provide relatively poor limits of detection, they are not suitable for low level determinations of indoor gaseous HCHO.[4]

Spectroscopic techniques that have been used to measure formaldehyde include differential optical absorption spectroscopy, Fourier transform infrared absorption, laser-induced fluorescence spectroscopy, and tunable diode laser absorption spectroscopy. Although these techniques are selective, non-destructive and quantitative allowing for

continuous detection, the requirement of large, complex, and expensive instrumentation makes these methods less attractive for routine applications.[32,33] In chromatographic methods, chemical derivatization is used for the determination of carbonyl compounds. The most commonly used derivatization method is based on the reaction of carbonyls with 2,4-dinitrophenylhydrazine (DNPH) to form the corresponding hydrazone derivatives, which are then separated by high performance liquid chromatography and detected by UV-Vis absorption.[34,35] Overall these methods generally take long sampling times and are not suitable for continuous analysis. Methods that utilize fluorescence detection are more sensitive and allow for continuous analysis. Techniques involving enzymes are very sensitive and selective, and have compared well in inter-comparison studies with other methods.[36] The major problem with these methods is that they are expensive, not very stable, and may precipitate out of solution which results in reduced response.[4]

1.3 LASERS:

Lasers are light sources that produce light amplification by stimulated emission of radiation. A typical laser produces light in a narrow, collimated beam over a small range of wavelengths. The term YAG laser is usually used for solid state lasers based on neodymium-doped YAG materials where YAG represents yttrium aluminum garnet. Nd:YAG lasers can be diode-pumped or lamp-pumped. Lamp pumping is possible due to the broadband absorption of the Nd:YAG material mainly in the 800 nm region. The fundamental Nd:YAG emission wavelength is 1064 nm in the infrared region. Starting

with that wavelength, outputs at 532 nm, 355 nm and 266 nm can be generated by frequency doubling, tripling and quadrupling process, respectively.[16]

1.4 LASER INDUCED FLUORESCENCE (LIF):

Fluorescence is the optical emission from molecules that are excited to higher energy levels by absorption of electromagnetic radiation from a light source. Laser-induced fluorescence (LIF) is a spectroscopic method that can be used for analyzing the electronic structure of molecules and their interactions, detection of selected species, and flow visualization and measurements. LIF is one of the most sensitive spectroscopic approaches available for analytical measurements. The main advantage of fluorescence measurements compared to absorption measurements is the high signal to noise which is possible because the fluorescence signal usually has a very low background. For molecules that can be resonantly excited, LIF allows selective excitation of the analyte that avoids interferences. Analytical applications of LIF include monitoring gas-phase concentrations in the atmosphere, flames, and plasmas, and remote sensing using light detection and ranging (LIDAR).[17]

In LIF experiments, a laser is used to excite an analyte molecule from a lower state to an excited state and, as it undergoes decay, fluorescence light is emitted. The intensity of fluorescence is directly proportional to the analyte concentration, and also may depend on gas temperature, pressure and the intensity of the light source.

Principle: LIF involves two steps, absorption and relaxation, as shown in Figure 1. When molecules absorb laser energy at a particular wavelength, they undergo excitation from the ground state to a higher energy (excited) state. In the excited state, molecules normally have greater vibrational energy than they had in the ground state. This extra vibrational energy may be lost by nonradiative processes, after which the molecules return to the ground state with the emission of light as fluorescence. For this reason, fluorescence emissions are often shifted to longer wavelengths that are lower in energy compared to the absorption wavelength.

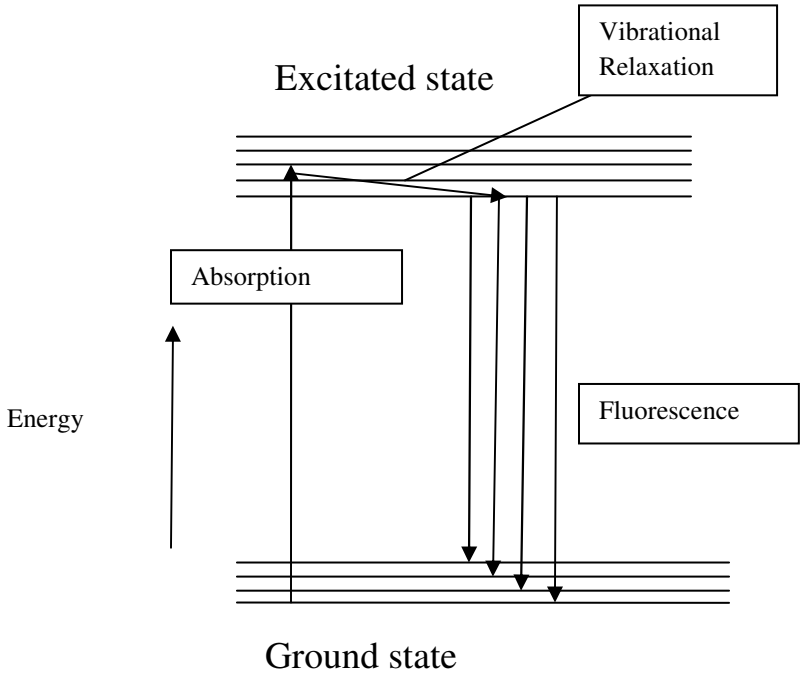

Figure 1 Principle of Fluorescence

1.5 HCHO Spectroscopy:

The absorption spectrum of formaldehyde in the near ultra-violet region consists of vibronic bands in the $A^1A_2 \leftarrow X^1A_2$ transition, which covers a wavelength range from

270 to 360 nm. As the temperature is increased, the absorption spectrum for formaldehyde becomes more complicated as higher vibrational states are populated.[3] The third harmonic Nd:YAG laser at 355 nm can be used for the excitation of formaldehyde at the long wavelength edge of the A ← X transition, as has been shown by previous works [15,37] as well as in these experiments. The advantage of using the Nd:YAG laser for LIF of formaldehyde is that it provides high pulse energy at 355 nm and is non-tunable, which means that it cannot be detuned. The main drawback with using this source is that it excites relatively weak rotational transitions in the molecule.[38]

1.6 LIF of HCHO:

The first measurements of formaldehyde in a flame using laser-induced fluorescence were reported by Harrington and Smyth.[38] They used a tunable dye laser for excitation at 352.48 nm.[7] Others have tried 353.2 nm [42,43,44] and 352.97 nm [44] where the absorption is also comparably weak. Some authors employed laser excitation at other bands such as at 339.23 nm [39] and 338.1 nm.[40] These wavelengths are accessible to XeF excimer lasers, which can reach high intensities, where saturation can take place for background fluorescence from polycyclic aromatic hydrocarbons (PAH) but not for formaldehyde.[38] This reduces the interference from PAH relative to the formaldehyde signal. Klein-Douwel *et al.*[45] proposed excitation by using the hot band 4_1^0, to reduce variation of the LIF signal due to changes in temperature. Absolute concentration measurements by use of LIF suffer from various types of quenching processes. A correction of LIF intensities for quenching can be obtained from fluorescence quantum yields.

1.7 HCHO at 355 nm:

For the detection of formaldehyde, the use of the third harmonic of a nontunable Nd:YAG laser at 355 nm as the excitation wavelength has previously shown good results. As reported previously, laser radiation at 355 nm involves the 4^1_0 band of the electronic transition $A^1 A_2 \leftarrow X^1 A_1$.[3] The fluorescence spectrum primarily shows a vibronic band progression starting in the 4^1 vibronic state.[3] The advantage of LIF at 355 nm is that a standard Nd:YAG laser can be used with high pulse energy. Previous studies have investigated the use of high laser power for potential occurrence of photochemical effects. In addition to this, studies have been performed of the photochemical processes which interfere with formaldehyde production or which result in species that interfere with the formaldehyde fluorescence spectrally.[7] The major disadvantage of excitation at 355 nm is a low absorption coefficient for HCHO and possible spectral interferences from other species such as PAH's during laser induced fluorescence measurements. Mohlmann had reported on the use of a 355 nm laser for detection of HCHO air. A limit of detection of 0.15 ppm was reported for HCHO in air.[15] Brackmann et al had reported on the use of 355 nm laser for HCHO detection in flame gases.[3]

1.8 Permeation Tube Sources:

Permeation devices are small, inert capsules that contain pure chemical compounds. These tubes provide the target compound in two phase equilibrium between its gas phase and its liquid or solid phase. The tubes provide constant emission of the compound at constant temperature. These tubes are useful for long term studies of effects of the compound on materials and on biological systems. A wide range of permeation

rates can be obtained by changing the length and width of the tube. The advantage of permeation tubes over gas cylinders are convenience, low expense and the ability to prepare mixtures simply by combining tubes.

In these studies, a tubular device as shown in Figure 2 has been used for formaldehyde. The device is one that contains the desired compound gas in a sealed Teflon tube. Release of the compound in the gas phase occurs by HCHO diffusion through the wall of the tube.[8]

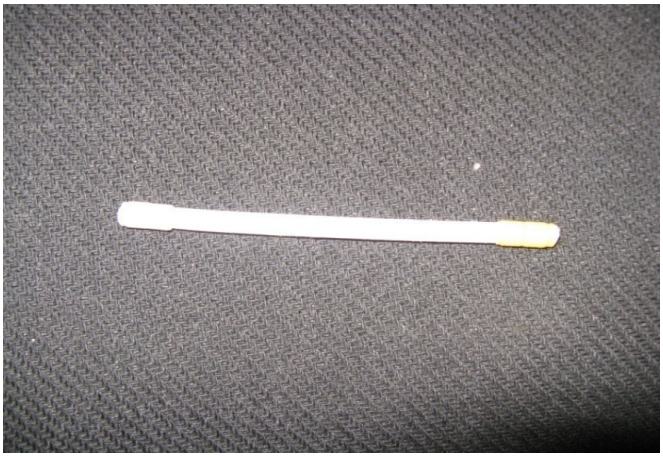

Figure 2 HCHO permeation tube

1.9 Raman Scattering:

Raman scattering, or the Raman effect, is the inelastic scattering of a photon. Inelastic scattering occurs when the energy of a photon is not conserved during the scattering process. During the scattering process, the incident photon either gains or loses energy. In Raman scattering, the incident photon interacts with a gas, liquid, or solid resulting in a change in the frequency of the photon. A blue shift is observed when the

internal energy of the matter is transferred to the photon and this process is called anti-Stokes Raman scattering. A red shift is observed when some of the energy of the photon is transferred to the material and this process is called Stokes Raman scattering. Both processes are shown in Figure 3. Scattering can occur with a change in vibrational, rotational, or electronic energy of the scattering molecule. In Raman scattering, the difference in energy between the incident and re-emitted photons often corresponds to the energy required to excite a molecule to a higher vibrational energy.

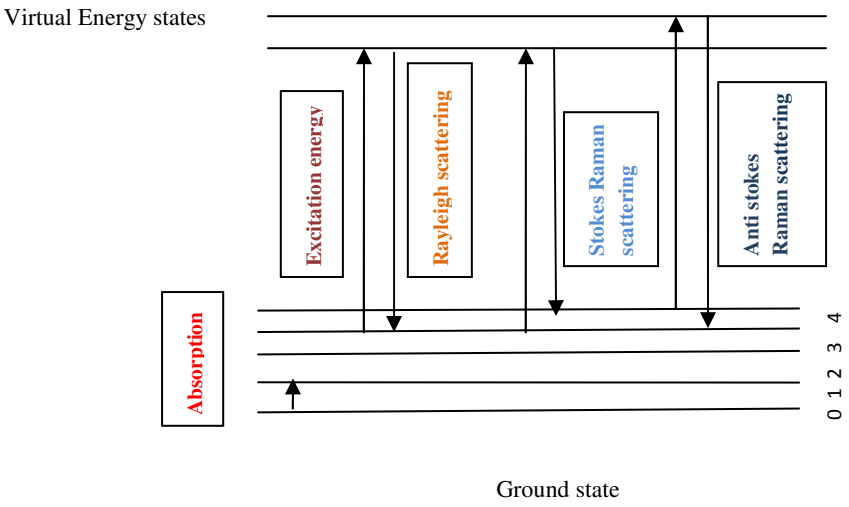

Figure 3 Principle of Raman scattering

1.10 Stimulated Raman scattering (SRS):

Stimulated Raman scattering (SRS) is a combination of the Raman effect with stimulated emission. It has been observed in solids, liquids, and gases.[16] It was first demonstrated by Woodbury, Ng [46] and Eckhardt *et al.*[47] in 1962. It is a process that is

useful for shifting narrow bandwidth laser radiation to different wavelengths and is able to provide high radiation fluxes at difficult to reach wavelengths. In SRS, the output radiation that is shifted by a four wave mixing process is coherent and as monochromatic as the initial pump laser beam. The tunability of the scattered Raman radiation depends on the tunability of the incident laser. If the pumping laser source is scanned in terms of wavelengths, the SRS generated radiation is scanned over a similar range.[9]

To achieve maximum radiant flux of a shifted wavelength, three experimental parameters are adjusted. These parameters include the power of the laser source, the pressure of the gas inside the SRS cell, and the absolute temperature of the scattering gas. The radiant flux of a shifted wavelength is directly proportional to the pump power, and is indirectly proportional to gas pressure because of an optical dispersion factor. The Raman conversion also depends on the gas temperature and is increased as the temperature is decreased because the Raman gain coefficient is a function of the reciprocal of the square root of temperature. Due to this dependence, greater radiant fluxes in the shifted wavelengths can be obtained at liquid nitrogen temperatures rather than room temperature for the same pump power.

Pumping lasers for SRS often include the second, third, and fourth harmonics of a Nd:YAG laser. Hydrogen, methane, and mixtures of these two gases can be used as a Raman medium. The harmonics provide pump frequencies in the visible, near UV, and far UV. Hydrogen, methane and mixtures of these two gases can be used because of their simple and strong stimulated Raman spectrum, their stability, and their transparency throughout the spectral region of interest. Hydrogen shifts the radiation by 4155 cm^{-1}

while methane shifts it by 2916 cm^{-1}, and mixtures of the two gases can produce several intermediate shift values.[13]

1.11 Optical filters:

An optical filter is a passive optical device that selectively transmits some optical radiation and blocks the rest. Depending on the type of blocking, filters are classified as long pass filters, short pass filters, neutral density filters, and band pass filters.

Long pass filter (LP): These filters attenuate shorter wavelengths and transmit longer wavelengths over a targeted range of the spectrum.

*Short pass filter (*SP): These filters attenuate longer wavelengths and transmit shorter wavelengths over a targeted range of the spectrum.

Band pass filter (BP): The combination of a long pass filter and a short pass filter results in a band pass filter. These filters usually have lower transmittance values than SP and LP filters, and block all wavelengths outside of a selected interval, which can be wide or narrow, depending on the bandpass interval.

Neutral Density filter: These filters have a nearly constant attenuation across a wide range of wavelengths. These filters are used to reduce the intensity of light by reflecting a portion of it. They are specified by the optical density, which is the negative of the logarithm of the transmission coefficient.

1.12 Detection Limits:

Detection limits are useful analytical figures of merit for comparing methods for a single species or for comparing several species by a single method. This helps one to make decisions as to which method should be considered useful and which should not be considered for a given application. The limit of detection (LOD) is the concentration at which one can decide whether an analyte is present or not, that is the point where one can distinguish a signal from the background.[18] According to the International Union of Pure and Applied Chemistry (IUPAC), the LOD is the concentration, $C_{L,}$ which is derived from the smallest measure, $X_{L,}$ which can be detected with reasonable certainty for a given analytical procedure.

$$X_L = X_{bi} + Ks_{bi} \qquad (6)$$

In the above expression, X_{bi} is the mean of the blank measurements, S_{bi} is the standard deviation of the blank measurements, and K is the numerical factor chosen according to the statistical confidence level.

If the measurement $X_{L,}$ is converted to concentration, $C_{L,}$ then the above equation becomes the following

$$C_L = C_{bi} + Ks_{bi}/S \qquad (7)$$

where S is the slope of the calibration curve. As the concentration of the blank is zero the equation (7) becomes

$$C_L = Ks_{bi}/S \qquad (8)$$

In these studies, K = 3 is used for calculating the LOD.[18]

2.0 Experimental Section:

2.1 Chemical:

Formaldehyde permeation tubes (VICI metronics Dynacal)

Specifications: Length: 11.8 cm

Rate: 6,136 ng/min at 100^{o}c

Type: HE

Permeation tubes are available in three types; Tubular devices, extended life tubular devices and wafer devices. In these studies, a tubular device for formaldehyde was used. The tubular device is one which contains the desired permeant gas in a sealed Teflon tube.

2.2 Apparatus:

The major components of the experimental setup for this study are listed in Table 1.

Table 1 Experimental components of LIF System

A. Laser System

Component	Model no.	Manufacture
Nd:YAG laser(355) non tunable	Surelite Laser II-10	Continuum
Raman Convertor 0.3m	PAL 101-RC	Light Age
Nd:YAG laser (non tunable)	GCR- 1A	Quanta-Ray

B. Optical Detection and Signal Processing

Photomultiplier tube	R 955	Hamamatsu
Monochromator (422.5nm)	1030	Jarrell Ash
Gated integrator & Boxcar Averager	SR 250	Stanford Research Systems
Oscilloscope	TDS 350 , Two channel, 200MHZ, 1GS/s	Tektronix

C. Sample Collection

Dynacalibrator	230	VICI metronics
HCHO Permeation tube	Tubular	VICI metronics

The specifications of Nd:YAG laser which is used in this study are listed in Table 2.

Table 2 Laser Specifications

Energies	SL-II- 10
355 nm	100/160 mJ
Repetition Rate (HZ)	10
Pulse width	4-6

2.3 Sample Preparation:

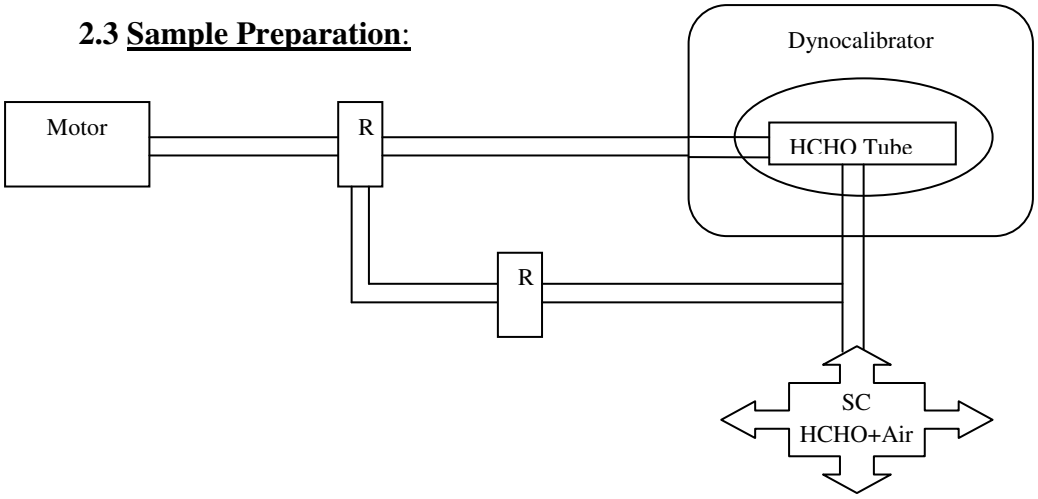

Figure 4 Schematic diagram of HCHO sample preparation; R represents the flow regulator, SC represents sample cell.

During this work, HCHO concentrations are obtained from a permeation tube having a permeation rate of 6136 ng/min at 100 ^{o}C. This permeation tube is placed in a dynacalibrator model 230, as shown in Figure 4. The highest concentration obtained from this system at 100 ^{o}C is 57.3 ppm and the lowest concentration obtained by dilution at 100 ^{o}C is 7.8 ppm.

2.4 Sample cells:

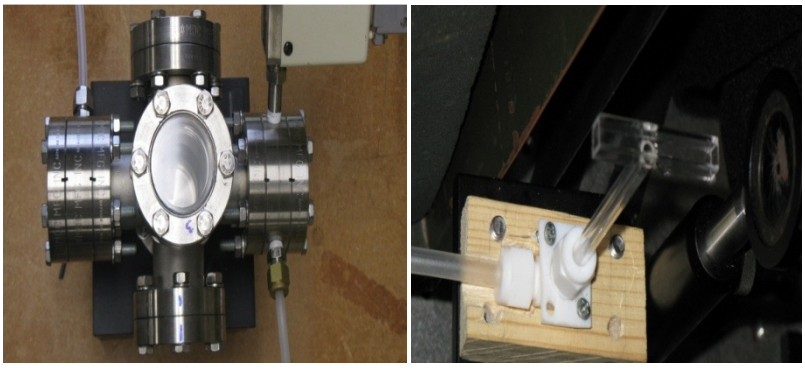

Figure 5 Types of sample cells used during this work; a) steel cell, b) T shape cell

a) Steel cell: This sample cell is a closed apparatus with quartz windows as shown in Figure 5(a). One consideration for this cell is it takes several minutes to change the concentration inside the cell. Another consideration is that as the cell windows are made of quartz, the laser passing through this cell can reflect off the window surfaces inside the cell.

b) T cell: It is an open cell made of uv-transparent quartz as shown in Figure 5(b). The advantage of the T cell when compared to the steel cell is, that it takes less time to make changes in concentration and there are no laser reflections from windows.

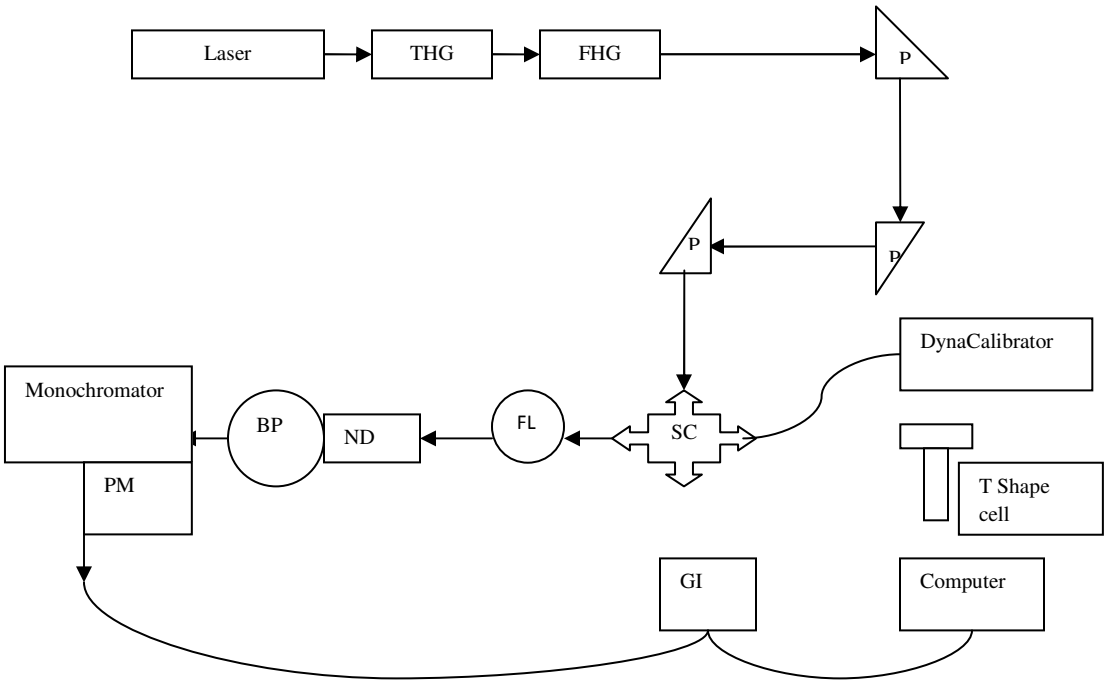

Figure 6 Schematic view of the experimental set- up: THG, third harmonic generator, FHG, fourth harmonic generator; P, prisms; SC, sample cell with quartz

windows; T shape cell, another type of sample cell; FL, focusing lens; ND, neutral density filter; BP, band pass filter; PM, photomultiplier; GI, gated integrator.

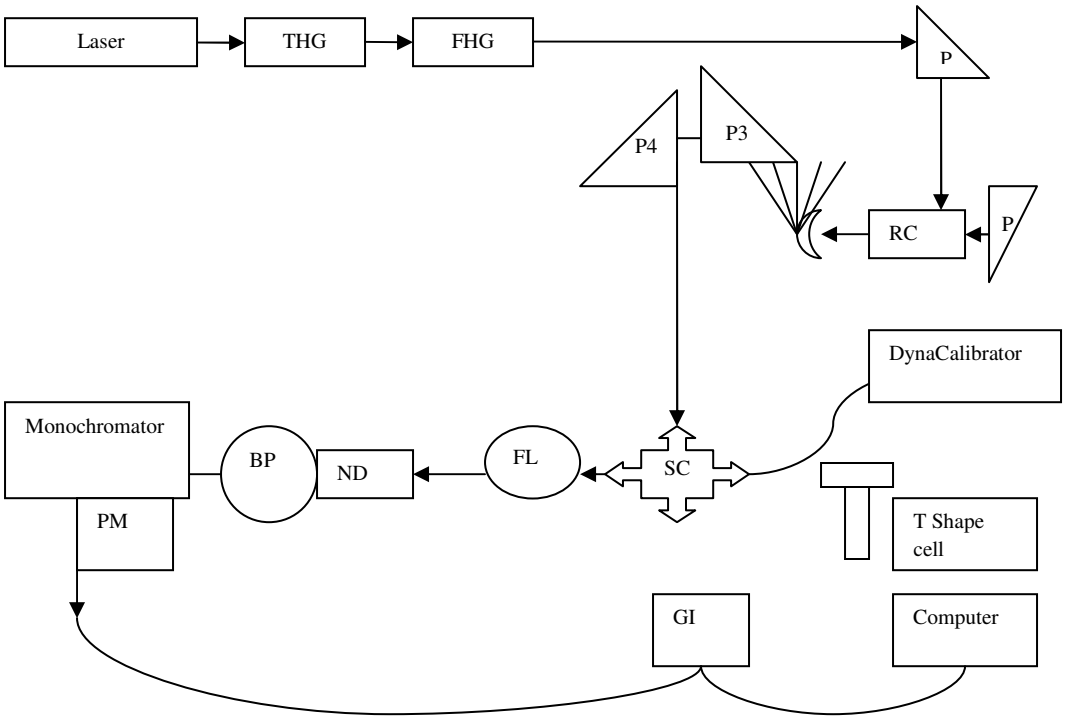

Figure 7 Schematic view of the experimental setup with Raman converter (RC).

The difference between Figure 6 and Figure 7 is a Raman shifter which produces different Raman-shifted wavelengths. The pump source is a pulsed Nd: YAG laser with a 1064 nm fundamental wavelength. The pump laser wavelength can be adjusted to different harmonics to get 532 nm, 355 nm, and 266 nm. In this work, the 355 nm and 266 nm were used as pumping wavelengths. The laser beam having the desired wavelength passed through the gas cell which is made of stainless steel and is a cylinder having dimensions of 75 cm long with a 1 cm inside diameter. Two right angle

deflections were used to direct the laser beam into and out of the Raman cell. The Raman cell was filled with high purity hydrogen with a pressure of 500 psi during this work. The laser outputs from the Raman cell consisted of pump, stokes and antistokes frequencies, and were directed to a Pellin-Broca prism positioned at the exit end of the Raman shifter. The desired output frequency of the Raman shifter was directed to prism (P3) and from there to Prism (P4). The prism (P4) was adjusted to align the laser beam with the entrance of the sample cell. In this work, the 309 nm Raman shifted wavelength was obtained from the 355 nm harmonic and the 341 nm Raman shifted wavelength was obtained from the 266 nm harmonic. These wavelengths were used in addition to 355 nm as excitation for LIF measurements of HCHO.

Procedure:

For the excitation of formaldehyde, the frequency tripled output of a Nd: YAG laser (nontunable) having a wavelength of 355 nm was used. The laser pulses were about 5 nanoseconds long and the laser pulse repetition frequency was 10 Hz. The 355 nm laser radiation was absorbed by the formaldehyde molecules and caused fluorescence from the same electronic band system. This fluorescence was detected by a monochromator-photomultiplier combination and the pulsed signals produced by the photomultiplier were fed into the input channel of a gated-integrator/boxcar-averager system. The time window of the gated integrator was chosen to be 13.5 nm for the detection of the fluorescence, and was synchronized to the laser excitation pulse. The sample cell contains a formaldehyde and air mixture which is obtained from a permeation tube device that is thermo regulated. As the temperature of the permeation tube is increased, the

formaldehyde concentration increases. The source for formaldehyde used is a formaldehyde tube which is in semi-solid form. A flow meter is used to control the air flow in order to conveniently produce different concentrations.

3.0 ***Results and Discussion***:

3.1 HCHO studies: The absorption of HCHO at 355 nm corresponds to the excitation of the $A^1A_2 \leftarrow X^1A_1$ transition and leads to fluorescence emissions ranging from approximately 390 nm- 600 nm. Shown in Figure 9 is the fluorescence emission spectrum for a HCHO/ air mixture when it is excited at 355 nm. The major peaks in the spectrum correspond to vibronic transitions from the excited state to the ground state. These transitions have been assigned previously.[38] The major bands observed in this spectrum are listed in Table 3.

Table 3 Major bands observed in Figure 9 and their intensities

Wavelength (nm)	**Relative Intensity**	**Assigned Transitions** [3]
409	1.2	$2^0_2 4^1_0$
416	1.75	$2^0_1 4^1_2$
425	2.4	4^1_4
435	2.1	$2^0_3 4^1_0$
445	1.45	$2^0_2 4^1_2$
455	1.6	$2^0_1 4^1_4$
465	1.5	$2^0_1 4^1_6 + 2^0_4 4^1_0$
480	1.25	

The spectrum in Figure 8 correlates well with the fluorescence spectrum of HCHO excited at 355 nm that has been reported previously.[38,15] According to the spectrum in Figure 8, the strongest fluorescence emission was observed near 425 nm.

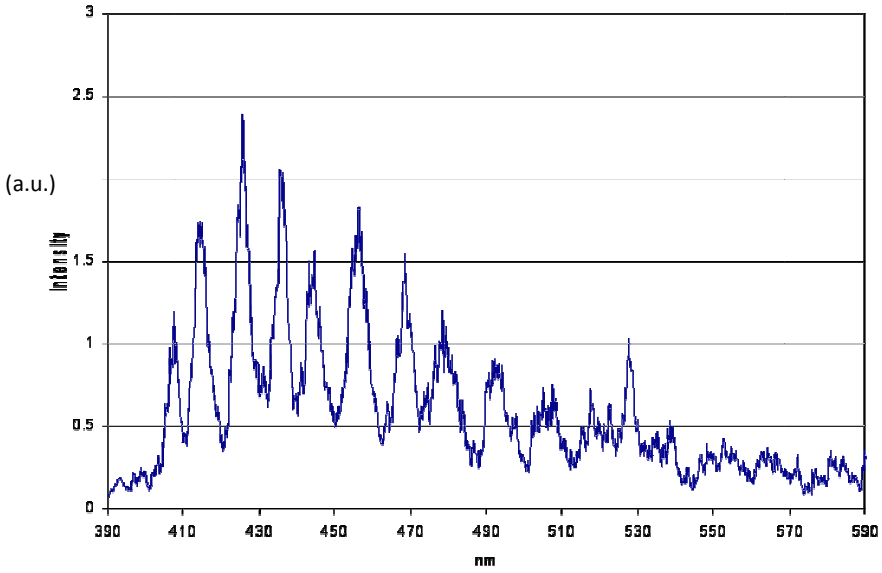

Figure 8 Fluorescence Spectrum of HCHO scanned from 390 nm- 600 using automated monochromator, with steel cell, Slit width 500 µm

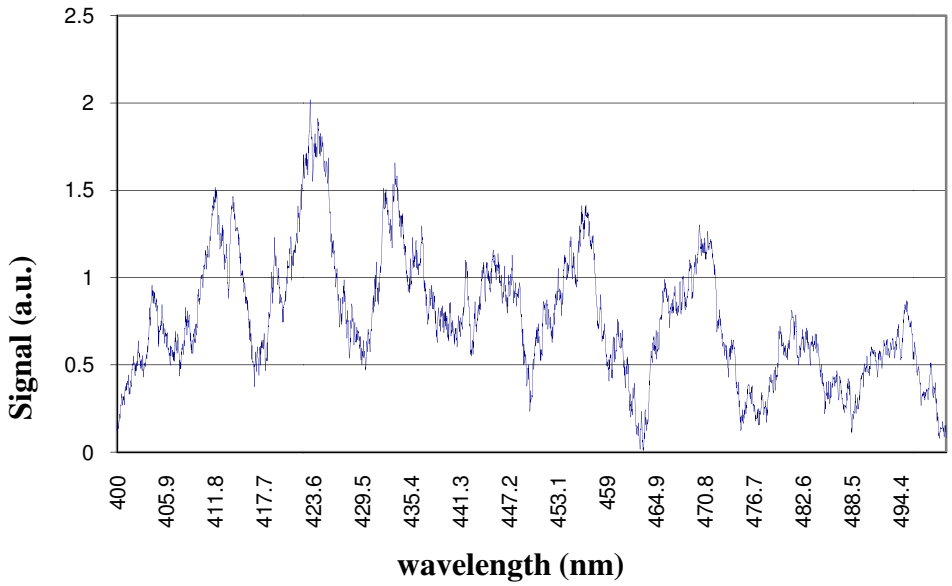

Figure 9 HCHO spectrum from 400-500 nm average 30, slit width 1000 µm, no focusing lens with T cell and high voltage of -1200V

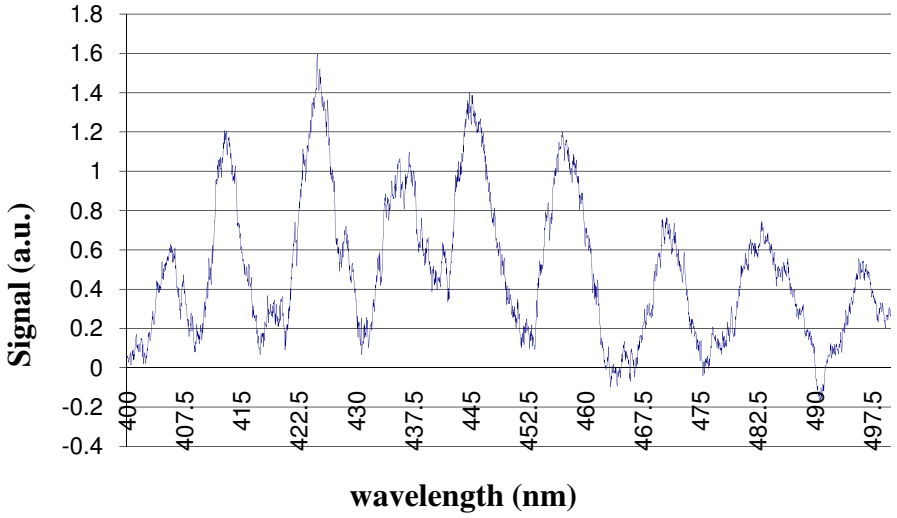

Figure 10 HCHO spectrum slit width 500 µm, average 30, -1100 V.

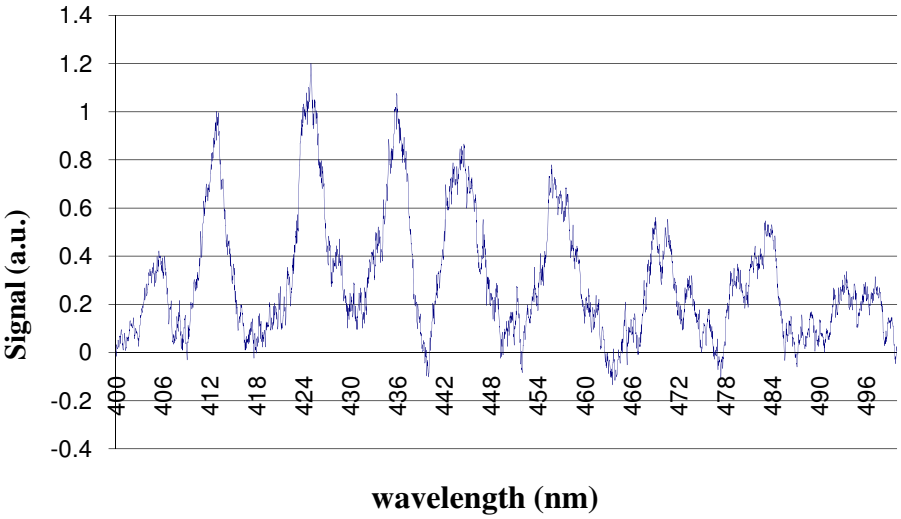

Figure 11 HCHO spectrum slit width 250 µm, average 30, -1200 V.

Shown in the Figures 9, 10, and 11 are LIF emission spectra for HCHO that were performed using the open T cell with no windows. These spectra show the same scan

using different monochromator slit widths. As the data show, the spectral features are the same as that of the spectrum obtained using the large closed cell, showing the strongest emission occurring at 425 nm. The spectra also show that decreasing the slit width improves the spectral resolution allowing near baseline resolution of the bands when using 250 µm slit width.

3.1 (a) <u>Power vs. Signal</u>: A plot of the fluorescence signal as a function of the laser energy can be used to evaluate the fluorescence excitation characteristics of a LIF application. If the laser energy is sufficiently large, it may be possible to achieve an excitation rate that exceeds the relaxation rate, at which point the excitation is said to be optically saturated. Figure 12 is a plot of the HCHO fluorescence intensity at 425 nm as a function of the laser pulse energy at 355 nm. As the laser pulse energy increases, the fluorescence signal increases. It is also noted that the fluorescence emission could be observed at laser energies as low as 0.5 mJ. The saturation point, where the observed signal is half its maximum value was not able to be determined in this case because the signal did not appear to reach a limiting value. This is important because it suggests that even stronger fluorescence signals can be achieved by using higher laser pulse energies that is by using a more powerful laser source.

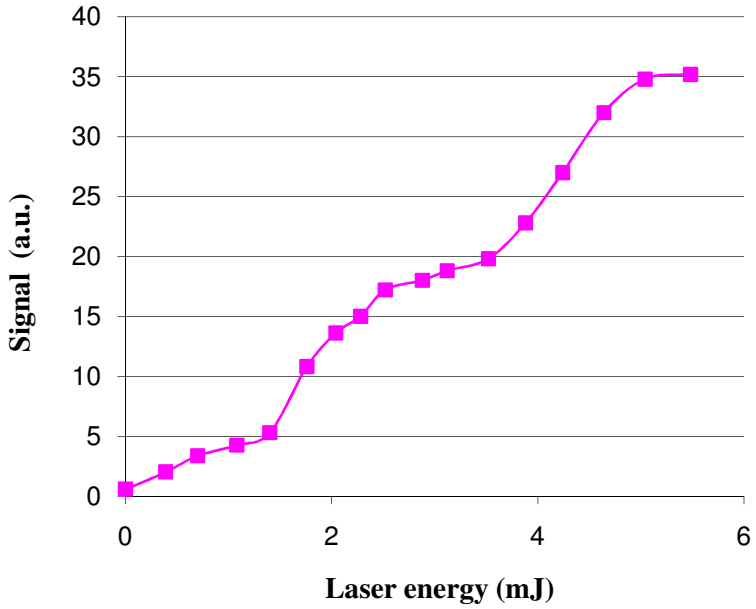

Figure 12 Fluorescence intensity vs. Laser energy using closed cell, Temperature 100 ^{0}C.

Figure 13 shows the power dependence of the HCHO fluorescence emission at 425 nm using a laser at 355 nm and a "T" cell as the sample cell. As in the closed cell, the fluorescence emission is observed to increase with laser energy and does not appear to saturate. This indicates that stronger fluorescence signals may be achieved using higher laser pulse energies. However, as the data in Figure 13 show, higher laser pulse energies are also likely to increase the background signal and may actually lower the signal to background ratio.

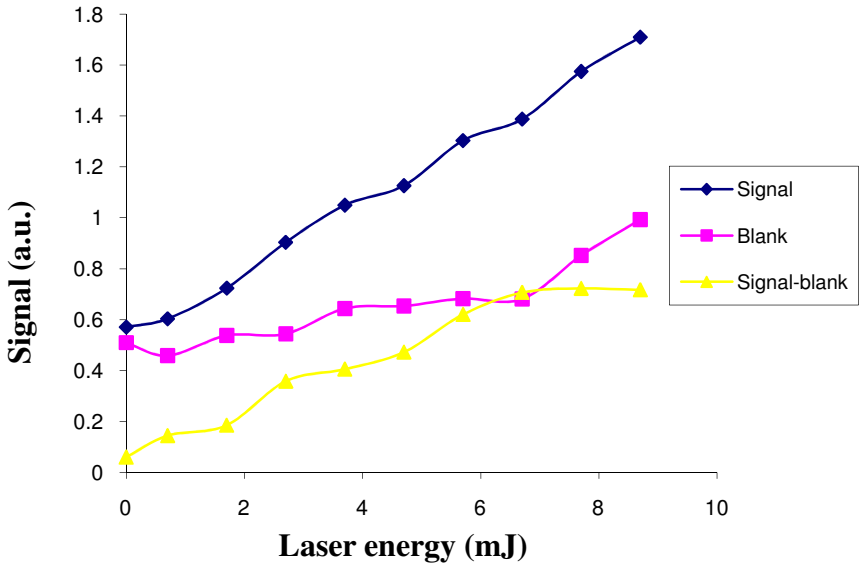

Figure 13 Fluorescence vs. Laser energy with T-cell, ND filter 1.0, average 300.

3.1 (b) <u>Signal vs. Noise</u>: Due to problems with the automated monochromator, it was necessary to use an alternative monochromator that was manual and not automated. In order to optimize the detection of HCHO with this monochromator, a signal to noise study was performed as a function of the fluorescence wavelength. In these measurements, the signal was defined as the signal produced by the analyte and the noise was defined as the standard deviation of several blank measurements without the analyte. As seen in Figure 14, the highest signal to noise was observed at a fluorescence wavelength of 425 nm using the alternative manual monochromator.

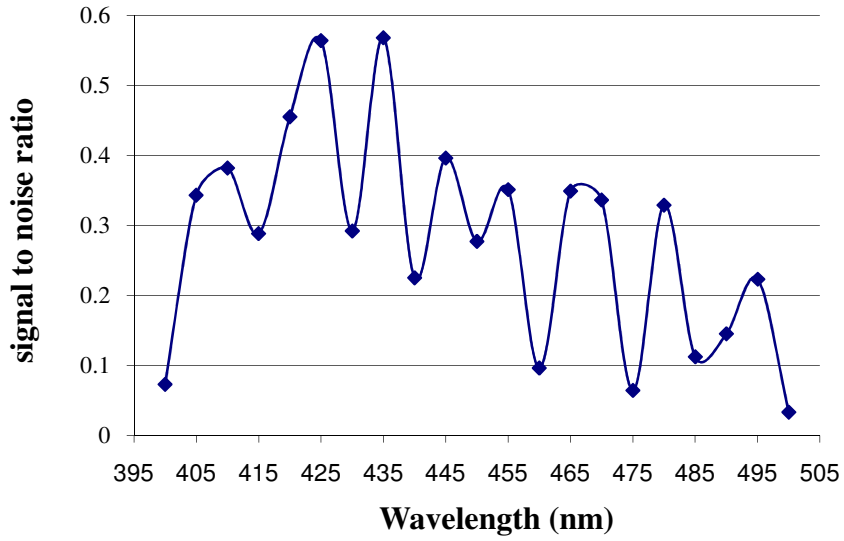

Figure 14 Signal to noise vs. fluorescence emission wavelength**.**

The major source for noise in these measurements is believed to be variations in the laser scatter from the cell windows in the closed cell as well as background fluorescence.

3.1 (c) <u>Analytical Measurements</u>: Once the optimum wavelength for fluorescence detection was determined, measurements were performed to evaluate the analytical utility of the fluorescence approach in terms of linearity and sensitivity. The HCHO permeation rate was 6136 ng/min at 100 ^{o}C and using different flows of air, the calibration response was evaluated in the range of 1-57 ppm HCHO.

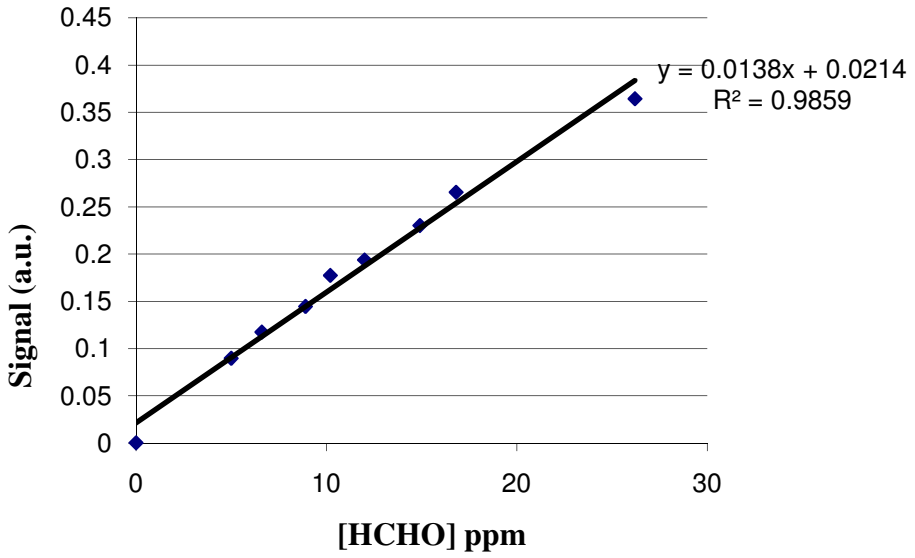

Figure 15 Calibration curve at 422.5 nm at temperature 90 ^{o}C.

Shown in Figure 15 is a typical calibration curve of HCHO obtained using the manual monochromator with averaging of 300 laser pulses. As the data indicate, there is very good linearity in the response as a function of HCHO concentration. However there is a significant fluorescence signal for the blank and it is the noise in the blank that determines the LOD. The LOD obtained in this case is 2 ppm.

Table 4 Parameters for calibration of HCHO using 355 nm as excitation wavelength with manual monochromator at 422.5 nm, gain 5mV/V, and the closed steel cell.

Laser Energy (mJ)	***Temp (oC)***	***Slit Width (µm)***	***Averaging***	***Volt (V)***	***LOD (ppm)***	***r2***	***Std.dev***
4.0	90	1000	30	-1100	5.04	0.983	0.020
4.08	90	1000	300	-1100	2.15	0.986	0.0098
4.0	90	1000	300	-1100	2.74	0.925	0.012
4.0	90	1000	300	-1100	4.24	0.986	0.017
4.04	90	1000	3000	-1100	1.93	0.994	0.007

The data in Table 4 show that increasing the averaging lowers the standard deviation which in turn lowers the LOD. However, increasing the averaging also increases the measurement response time. Most of the studies were performed at an averaging of 300 laser pulses as a compromise between low noise and long response times. Similar studies were conducted using the scanning monochromator Figure 16. Table 5 summarizes some of these results.

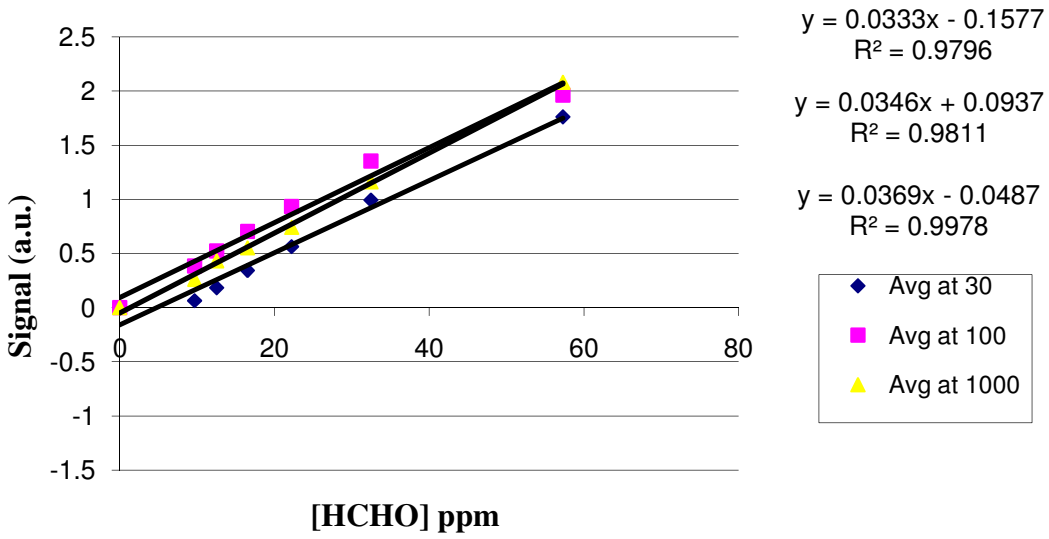

Figure 16 Calibration curve of HCHO at 425.6 nm, with the automated monochromator and averaging at 30, 100, 1000 laser pulses.

Table 5 Parameters for calibration of HCHO using 355 nm laser excitation and fluorescence detection at 425.6 nm with the automated monochromator and closed steel cell.

Laser Energy (mJ)	***Temp (oC)***	***Slit width (µm)***	***Averaging***	***Volt (V)***	***LOD (ppm)***	***r2***	***Std. dev***
9.0	100	1000	30	-1200	6.69	0.985	0.072
9.0	100	1000	30	-1200	5.78	0.979	0.065
9.0	100	1000	100	-1200	3.67	0.976	0.043
9.2	100	1000	100	-1200	4.69	0.982	0.054
9.0	100	1000	300	-1200	4.15	0.986	0.047
9.0	100	1000	1000	-1200	1.02	0.993	0.012

As the data in Table 5 indicate, there were similar results obtained using either monochromator system. In both cases, an increase in the averaging generally lowers the standard deviation and improves the limit of detection.

Due to the high background observed using the closed cell, an alternative sample cell was used that was open, i.e. without any windows. Figure 17 shows the calibration data of HCHO using the open "T" cell and the manual monochromator at different temperatures for the permeation tube (100 ^{o}C and 90 ^{o}C). The LOD obtained with this system is 0.5 ppm at 90 ^{o}C. This is the lowest limit of detection obtained during this work and indicates that using an open sample cell is preferable due to the lower background (Table 6). It is worth nothing from the two data series in Figure 17 that changing the temperature of the permeation tube shifts the HCHO concentrations but does not change the fluorescence response or slope when all other conditions are held constant.

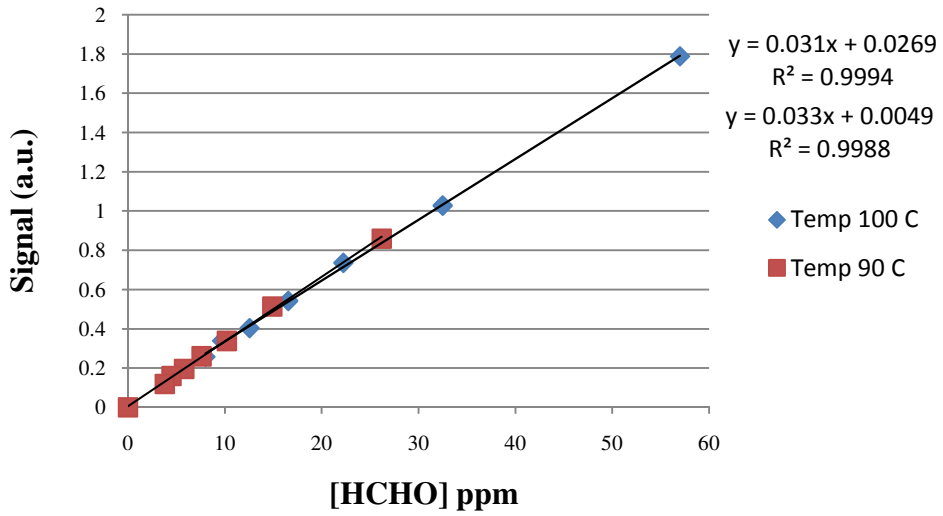

Figure 17 Calibration curve of HCHO at different temperatures using the T -cell and the manual monochromator.

Table 6 Parameters for calibration of HCHO using 355 nm as the excitation wavelength from the GCR laser with a focusing lens and fluorescence detection at 425 nm with the manual monochromator and the "T" cell

Laser energy (mJ)	***Temp (oC)***	***Slit width (μm)***	***ND filter***	***Averaging***	***Volt (V)***	***LOD (ppm)***	***Std. dev***	***r2***
8.4	100	1000	1.0	300	-1200	1.1	0.01	0.996
8.4	100	1000	1.0	300	-1200	1.6	0.01	0.999
8.4	90	1000	1.0	300	-1200	3.0	0.01	0.978
8.4	90	1000	1.0	300	-1200	0.5	0.05	0.999

3.1 (d) <u>Optical filters and PMT</u>: In order to further increase the sensitivity and lower the limit of detection, an alternative approach was used where the monochromator and PMT were replaced by a simple optical filter and PMT arrangement. The optical filters used were band pass filters that allow a narrow range of wavelengths to pass while blocking other wavelengths. Band pass filters were chosen that overlapped or nearly overlapped strong fluorescence emission bands of HCHO. For example, a band pass filter centered near 405 nm nearly overlaps the $2^0_2\,4^1_0$ fluorescence band at 409 nm as shown in Figure 18. A second band pass filter centered at 420 nm nearly overlaps the band 4^1_4 at 425 nm as shown in Figure 20. Shown in Figure 19 is the calibration of HCHO using the open "T" cell and a bandpass filter (405 nm) with a PMT. Although the sensitivity is much higher than that obtained using a monochromator, the background is also high and the

overall limit of detection is not improved. The LOD obtained under these conditions is 2 ppm. Further investigation is needed to improve this approach.

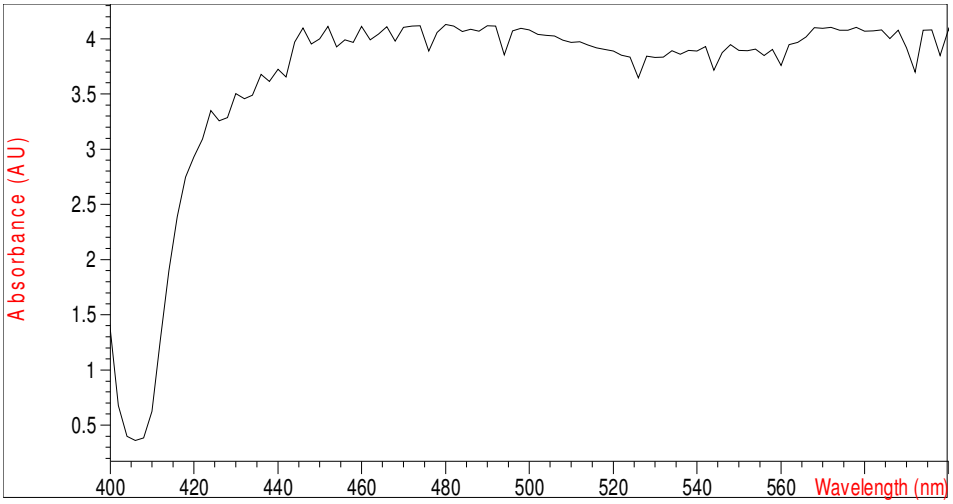

Figure 18 Transmission spectrum of the 405 nm band pass filter.

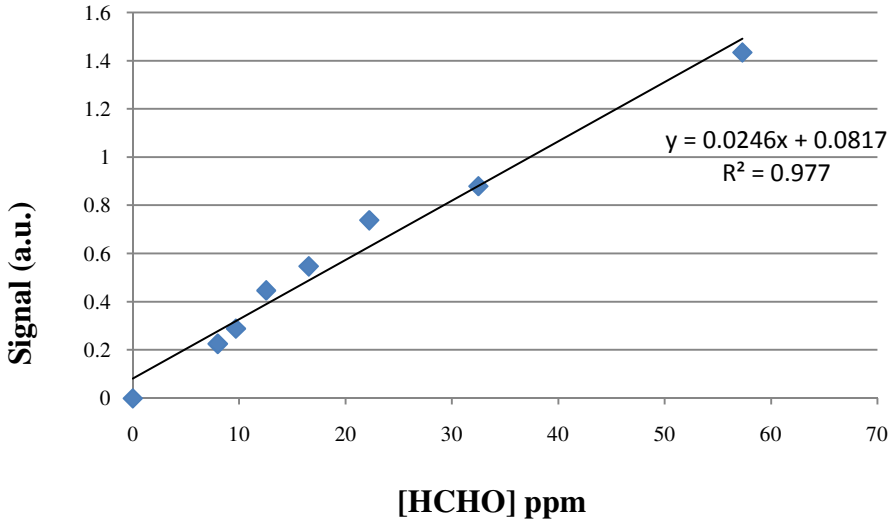

Figure 19 Calibration of HCHO using 355nm laser excitation, ND filter 2.0, average 300, temp 100° C, high voltage -1100 v, laser energy 8.4 mJ, using detector and filter with 'T' cell and 405 nm bandpass filter.

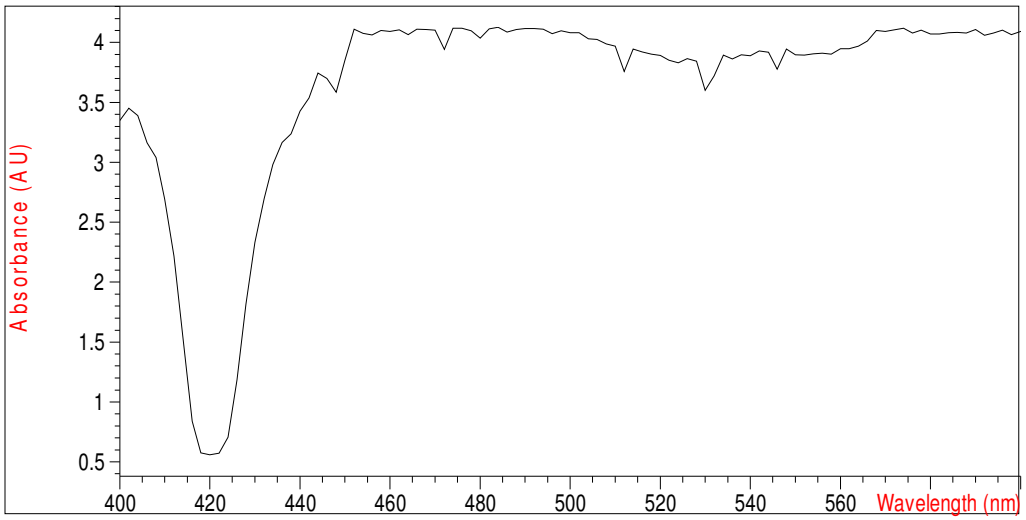

Figure 20 Transmission spectrum of 420 nm band pass filter.

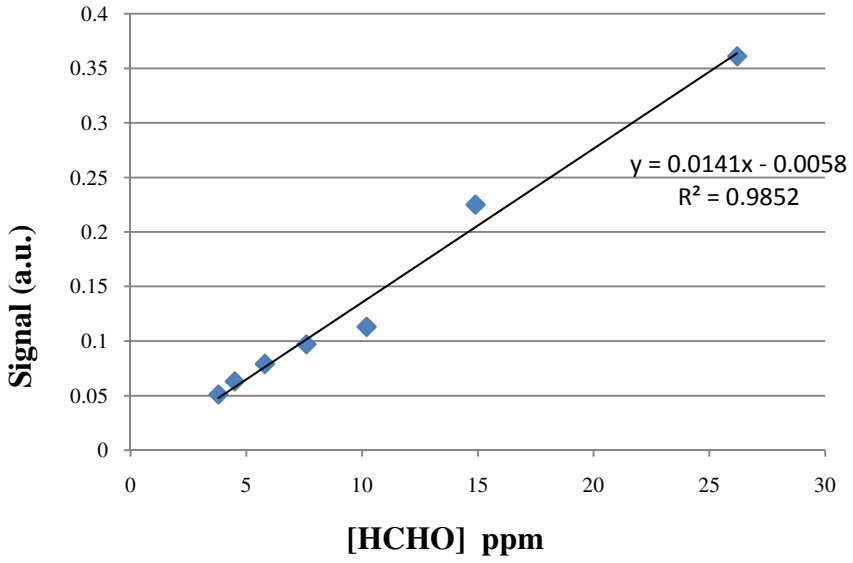

Figure 21 HCHO calibration curve using 355 nm laser excitation, average 300, N.D 2.0 filter, focusing lens with 'T' cell and 420 nm bandpass filter.

Although the sensitivity is much higher using the bandpass filter is much higher than that obtained with a monochromator, the background is also higher and the overall limit of

detection is not improved. Shown in Figure 21 is the calibration curve of HCHO at 90 ^{o}C, using the T cell and a 420 nm bandpass optical filter with a PMT for detection. The LOD obtained under these conditions is 1.7 ppm. The parameters used in this case are listed in Table 7.

Table 7 Parameters for calibration of HCHO using 355 nm laser excitation from the GCR laser with focusing lens, with filters and the 'T' cell, and averaging at 300.

Laser energy (mJ)	***Temp (^{o}C)***	***Bandpass filter***	***ND filter***	***Signal***	***Volt (V)***	***LOD (ppm)***	***Std.dev***	***r2***
8.4	100	405 nm	2.0	10	-1100	2.4	0.019	0.977
8.4	90	420 nm	2.0	10	-1100	1.7	0.008	0.985

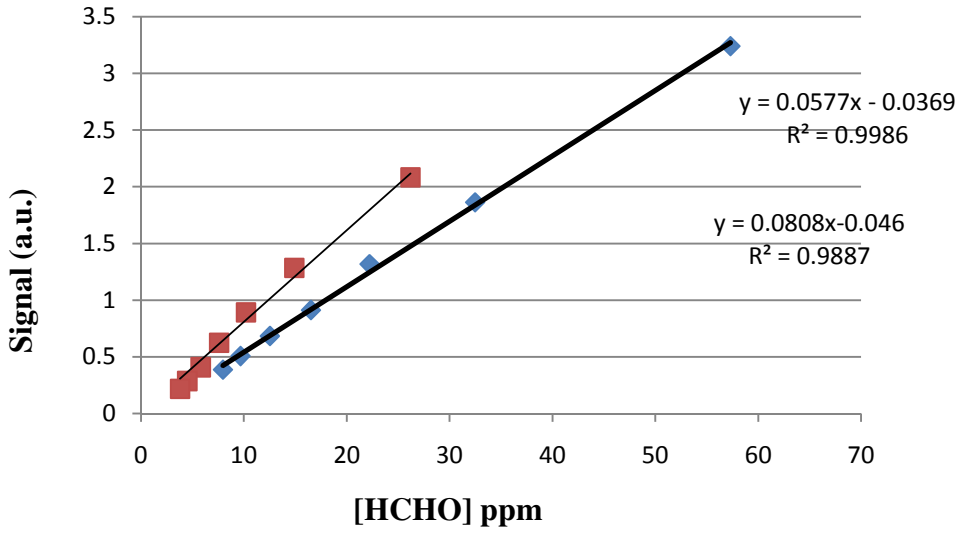

Figure 22 HCHO calibration curve using fluorescence detection at 424.13 nm, temperatures of 100^{o}C and 90^{o}C average 300, N.D 1.0, -1000 V, with focusing lens.

Shown in Figure 22 is the calibration curve of HCHO at temperatures 100 ^{o}C and 90 ^{o}C with the automated monochromator and the T cell. The parameters used in this case are listed in Table 8.

Table 8 Parameters for calibration of HCHO using 355 nm as the excitation wavelength from GCR laser with focusing lens, with automated monochromator and the T cell

Laser energy (mJ)	***Temp (^{o}C)***	***Slit width (µm)***	***ND filter***	***Volt (V)***	***Averaging***	***LOD (ppm)***	***Std.dev***	***r2***
8.4	100	1000	1.0	-1000	300	1.6	0.032	0.998
8.4	90	1000	1.0	-1000	300	1.6	0.0435	0.988
8.4	90	500		-1100	300	2.24	0.0248	0.999

Overall it is seen from the data shown in Figures 19, 21, 22 and Table 7 and 8 that the use of band pass filters did not improve the performance. Although the responses were higher using the filters, the background also increased and the overall signal to noise characteristics were not improved. This suggests that if better filters can be used, it may be possible to achieve higher signals without proportional increases in the noise and improved the signal to noise ratios.

3.2 <u>Raman Converter Studies</u>: It has been reported that HCHO absorbs light at several wavelengths in the range of 280 – 360 nm.[10] While the excitation at 355 nm has been used successfully for LIF detection of HCHO, there are other strong absorption bands in the $A^1A_2 \leftarrow X^1A_1$ transition that are also potentially useful. It is possible to produce wavelengths that overlap some of these bands by using

Stimulated Raman Scattering of non-tunable radiation from the Nd:YAG laser source. In the following studies, the production of alternative excitation wavelengths for LIF measurements of HCHO has been performed and the analytical performance of LIF approaches using these wavelengths has been investigated.

3.2 (a) H_2 SRS 266 nm for HCHO:

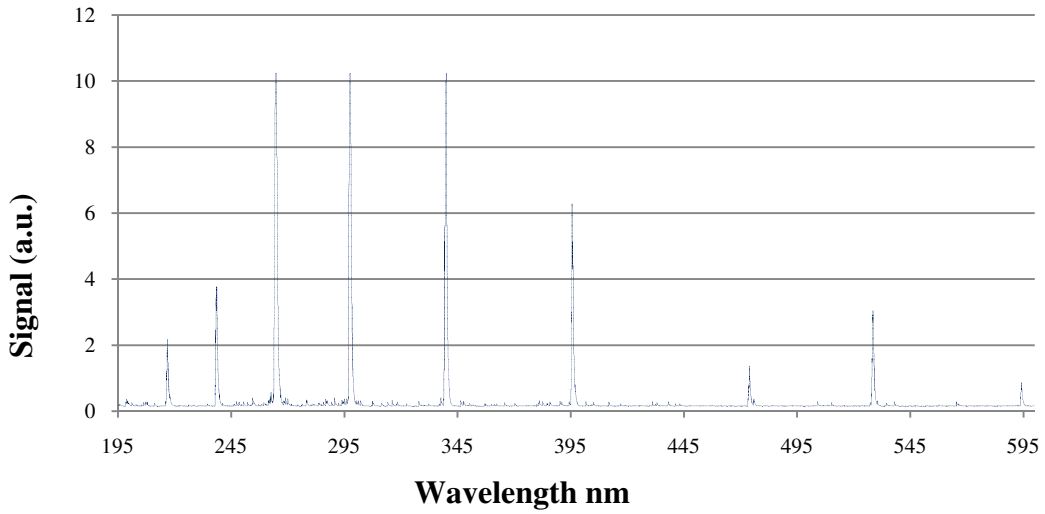

Figure 23 Scan of the outputs from the SRS cell using UV 266 nm laser radiation and hydrogen gas

Shown in Figure 23 are the 9 SRS outputs from the Raman Converter using the fourth harmonic of the Nd: YAG laser (266 nm) as the source wavelength. In this case, the Raman Converter is filled with H_2 gas at 500 psi. The laser emissions from the Raman cell are scanned with a monochromator from 195 nm – 600 nm. The outputs obtained in this case show good agreement with outputs reported earlier.[13]

From HCHO absorption spectra, it is expected that HCHO will undergo absorption at wavelengths of 341 nm and 309 nm.[10,12,48] The strength of the absorption band at 341 nm is approximately twice as strong as the absorption band at 309 nm.[48] By comparison, the absorption strength at 309 nm is only slightly higher than absorption at 355 nm.[48] In this work, 341 nm as well as 309 nm have been used as excitation sources for LIF measurements of HCHO. The results obtained with the 341 nm excitation show fluorescence spectra similar to the spectra obtained using 355 nm excitation where the maximum intensity is observed at 425 nm. The fluorescence spectrum for HCHO obtained with 341 nm excitation is shown in Figure 24.

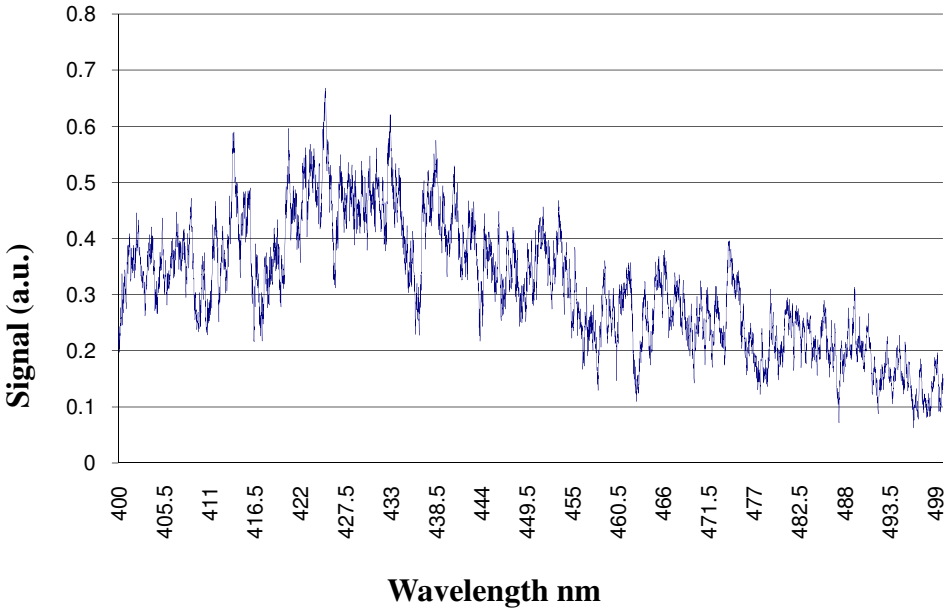

Figure 24 HCHO spectra at 341 nm, slit width 1000, average 30, -1200 V

Although the fluorescence emissions using 341 nm excitation are not as strong and not as well resolved as when using 355 nm excitation, it is important to note that the laser

energy at 341 nm is much less than at 355 nm. Since the fluorescence intensity is proportional to the source intensity, it is anticipated that the use of the same laser energy at 341 nm and 355 nm is expected to produce fluorescence emissions that are approximately 400 times larger than that obtained using 355 nm excitation. It should also be noted that the weaker fluorescence observed using 341 nm excitation may also be due to HCHO photofragmentation, which may reduce the fluorescence emission intensity.[12]

3.2 (b) H_2 SRS 355 for HCHO:

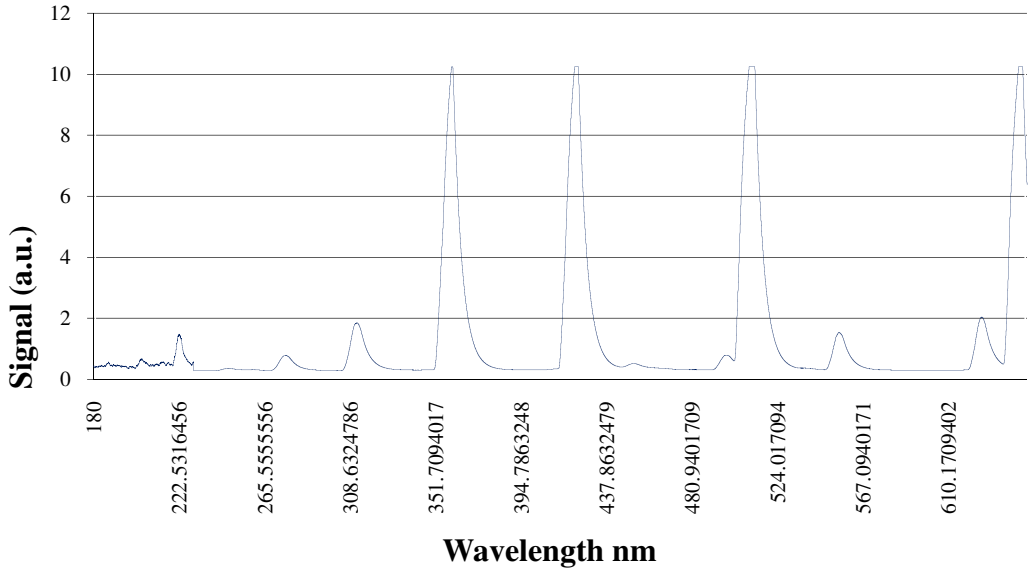

Figure 25 Scan outputs of 355 nm laser from 180-650 nm using Raman Convertor with hydrogen gas

Shown in Figure 25 are the 9 SRS outputs of the Raman Converter using the third harmonic Nd: YAG laser (355 nm) as the pump laser. In this case, the Raman Converter is filled with H_2 gas at 500 psi. The monochromator was scanned from 180 nm – 650 nm.

The outputs obtained in this case show good agreement with the outputs reported earlier.[13]

From previous reports, it was anticipated that LIF could be performed using laser excitation near 309 nm produced by Raman shifting of 355 nm.[10,12] In this case, the laser light was directed to the sample cell containing 57 ppm of HCHO and a fluorescence spectrum was recorded from 400 – 500 nm. The LIF spectrum shown in Figure 26 was taken with the manual monochromator. This spectrum shows large signals near 416 nm and 503 nm. These wavelengths appear to be scattering of light from the Raman Converter along with the 309 nm light (see Table 10). To overcome this problem, a spectrum was taken over a smaller wavelength range using the automated monochromator. The LIF spectrum using the automated monochromator at 309 nm is shown in Figure 27. As seen in Figures 26 and 27, LIF spectra using excitation at 309 nm show relatively weak fluorescence when compared to excitation at 355 nm. The weak fluorescence response may be due to low laser energy at 309 nm (see Table 10) and may also be due to photo-fragmentation of HCHO.[12]

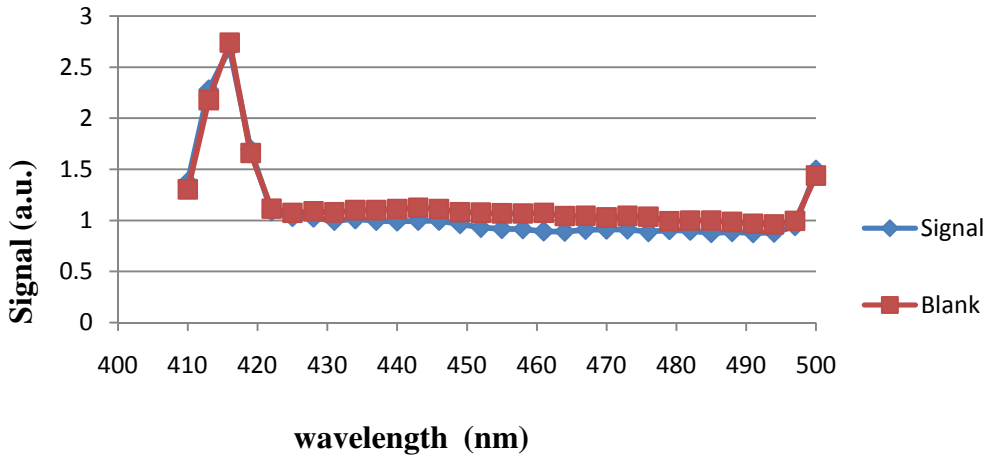

Figure 26 Spectrum of HCHO with manual monochromator using laser excitation at 309 nm, at -1200 V average at 300.

It is worth noting that the laser pulse energy at 309 nm is approximately 100 times smaller than at 355 nm. If the same laser energies are used at both wavelengths, it is expected that the fluorescence intensity will be 200 times larger using 309 nm excitation.

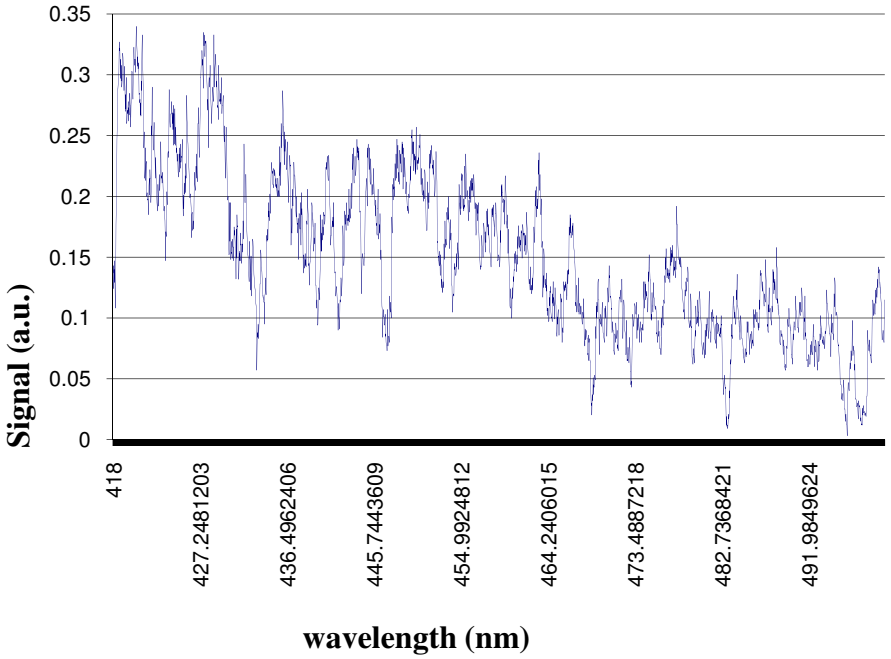

Figure 27 Spectrum of HCHO using 309 nm, slit width 1000, average 30, -1200 V.

3.2 (c) H_2 SRS 266 nm Conversion efficiencies:

To assess the efficiency of the SRS approach used in these studies, the Stimulated Raman Conversion efficiencies in hydrogen with 266 nm were measured. Table 9 shows the relative efficiency of outputs of 266 nm from the Raman Convertor. The measured conversion efficiencies indicate that the laser energy at 341 nm is much lower when compared to the 355 nm. As already discussed, it is anticipated that an increase in the laser energy at 341 nm could increase the fluorescence signals and LIF sensitivity proportionally.

Table 9 Relative Conversion efficiencies of outputs of 266 nm

Wavelength (nm)	***Energy mJ***	***% Relative conversion efficiency***
594.566	0.00013	0.013
476.78	0.008	0.11
397.9	0.105	1.5
341.48	0.256	3.6
299	0.167	2.4
266	0.231	3.3
239.5	0.033	0.5
217.58	0.013	0.2
199.76	0.001	0.01

266 nm energy in front of the convertor – 11.6 mJ

Energy behind the convertor – 7.1 mJ

3.2 (d) H_2 SRS 355 nm Conversion efficiencies:

The Stimulated Raman Conversion efficiencies in hydrogen with 355 nm have also been performed. Table 10 shows the efficiency of outputs of 355 nm from Raman Converter. The measured conversion efficiencies indicate that the laser energy near 309 nm is much lower compared to 355 nm. As discussed previously, it is anticipated that an increase in the laser energy at 309 nm will increase the fluorescence signals and the sensitivities for LIF detection of HCHO proportionally.

Table 10 Relative Conversion efficiencies of outputs of 355 nm

Wavelength (nm)	***Energy mJ***	***% Relative conversion efficiency***
636.2	0.9	7.5
503.2	1.05	8.75
416.2	0.5	4.16
354.8	0.4	3.33
309.0	0.08	0.66
274.0	0.06	0.5
246.0	0.016	0.13
223.2	0.00224	0.02
204.2	0.000245	0.002

355 nm energy in front of the convertor – 18.0 mJ

Energy behind the convertor – 12.0 mJ

3.2 (e) <u>Comparison of results to other LIF and Non- LIF approaches</u>:

A comparison of the performance characteristics of several HCHO measurement approaches is presented in Table 11. The performance of the current system in terms of the detection limit is not as good as those reported by most other approaches but is comparable to the other LIF technique reported previously by G. R. Mohlmann (1985).[15] Although the limit of detection in this work is approximately 3 times higher than that reported by Mohlmann (1985), [15] it is worth noting that the laser energies were also 3

times lower in this work. When this is accounted for, the two results are essentially the same assuming that the fluorescence is proportional to the source intensity.

Table 11 Comparison of experimental methods for HCHO detection

Technique	***Detection limit/ppb***	***Response/ Measurement time h^{-1}***	***Sample type***	***Refs.***
Tunable diode laser absorption spectroscopy	0.055	60	NA	Fried et al. (1999),[23] Cardenas et al. (2000) [22]
GC/HID (Gas chromatography/ Helium ionized detector)	0.042	11	NA	J. R. Hopkins *et al.* (2003) [20]
Fluorimetry (2,4-Pentadione)	1.6	30	Preconcentrated	Kamil Motyka *et al.* (2004) [4]
Girards' reagent/ Adsorption Voltammetry	0.7	120	Preconcentrated	Wing Hong Chan *et al*. (1997) [1]
Chemiluminescence based on Trautz-Schorigin Reaction	0.49	140	Preconcentrated	Kamil Motyka *et al.* (2006) [2]
LIF	150	30	NA	G. R. Mohlmann *et al.* (1985) [15]
This technique	500	20	NA	This work

When comparing the LIF approach to other techniques, there are some advantages to the LIF approach. For instance, in most of the other techniques, the air sample is collected and preconcentrated. In the case of LIF, the sample is not preconcentrated and the measurements are performed directly. Furthermore, the direct LIF approach using 355 nm laser excitation does not require the use of any reagents which can be unstable, expensive and/or hazardous. As a result, the direct LIF approach

is relatively uncomplicated and better suited to field measurements and potentially has better feasibility for remote or unattended measurements. Although the limit of detection reported here is not yet comparable to the other methods, it is anticipated that the use of higher pulse repetition rates and better bandpass filters will provide improved measurement capabilities for HCHO. It is also worth noting that not all HCHO monitoring applications require very high sensitivity. In such cases, a LIF sensor that is simple, direct and able to respond to ppm and even sub-ppm concentrations may be useful.

4.0 Conclusions:

These studies have shown that formaldehyde (HCHO) can be detected directly in air by laser induced fluorescence (LIF) using a non-tunable laser source. In this case, the third harmonic output of a nontunable Nd: YAG laser operating at 355 nm overlaps with a known HCHO absorption wavelength and is used directly as the excitation source. Since the laser is nontunable, the approach is simple to use because there is no chance for the laser to be detuned or lose wavelength calibration. Measurements are performed directly on air samples without preconcentration, which reduces the complexity of the approach and eliminates the need for reagents or other sample preparation steps. Several different configurations of sample cells, detection configurations and excitation wavelengths have been investigated in these studies. The lowest limit of detection of 0.5 ppm was obtained using 355 nm excitation with an open sample cell and a monochromator and PMT detection system. It is anticipated that for HCHO monitoring applications that do not require very high sensitivity or low detection limits, a simple, fast and direct fluorescence approach that can indicate potentially hazardous exposures HCHO at the low ppm level may be useful.

5.0 Further Studies:

In future studies, it would be of interest to investigate the following to improve the fluorescence approach.

1. Decreasing the background in the T- cell approach where optical filters are used instead of a monochromator.
2. Study of fiber optics, to simplify the delivery of the laser to the sample cell.
3. Performing better studies at 309 nm as well as 341 nm.
4. Performing spectral interference studies at 355 nm, 309nm, and 341 nm.
5. Study of Raman shifts with methane gas, as well as mixture of methane and hydrogen instead of hydrogen gas using both the third harmonic at 355 nm laser and fourth harmonic at 266 nm of the Nd: YAG laser.

6.0 References:

1. Wing Hong Chan, Tian Yao Xie*, Analytica Chimica Acta*, **1997**, 349, 349-357.
2. Kamil Motyka, Pavel Mikuska, Zybnek Vecera, *Analytica Chimica Acta,* **2006**, 562, 236-244.
3. C. Brackmann, J. Nygren, X. Bai, Z. Li, H. Bladh, B. Axelsson, I. Denbratt, L. Koopmans, Per-Erik. Bengtsson, M. Alden*, Spectrochimica Acta Part* A*,* **2003,** 59**,** 3347.
4. Kamil Motyka, Pavel Mikuska, A*nalytica Chimica Acta,* **2004**, 518, 51-57.
5. E. Priha, *Appl. Occup. Environ. Hyg,* **1996**, 11, 465-470.
6. www.atsdr.cdc.gov/toxprofiles/tp111-c6.pdf.
7. T. Metz, Xiao Bai, Frederik Ossler, Marcus Alden, *Spectrochimica Acta Part* A*,* **2004**, 60, 1043-1053.
8. www.vici.com/calib/permtube.pdf.
9. M. B. Leong, A. P. D Silva, V. A. Fassel, *Analytical Chemistry,* **1986**, 58, 13.
10. Chris A. Cantrell, James A. Davidson, Anthon H. McDaniel, Richard E. Shetter, Jack G. Calvert, *Journal of Physical Chemistry,* **1990**, 94, 3902-3908.
11. G. K Moorgat, Peter Warneck, *J. Chem. Physics*, **1979**, 70, 3639-3651.
12. R. G. Miller, E. K. C. Lee, *J. Chem. Physics*, **1978**, 68, 4448-4464.
13. George B. Jarvis, Sam Mathew, Jonathan E. Kenny, *Applied Optics*, **1994**, 33, 4938-4946.
14. Angleica Pretto, Marico R. Milani, Arnaldo A. Cardaso, *Journal of Environmental Monitoring*, **2000**, 2, 566-570.
15. G. R. Mohlmann, *Applied Spectroscopy*, **1985,** 39, 1, 98-101.

16. www.rp-photonics.com/yag_lasers.html.

17. www.chem.vt.edu/chem-ed/spec/laser/lif.html.

18. www.curvefit.com/linear_regression.html.

19. Volker Thomson, Debbie Schatzlein, David Mercuro*, Spectroscopy*, **2003**, 18, 12.

20. J. R. Hopkins, T. Still, S. Al-Haider, I. R. Fisher, A. C. Lewis, P. W. Seakins, *Atmospheric Environment,* **2003**, 37, 2557-2565.

21. Elisabete Alves Pereira, Emanuel Carrilho, Marina F. M. Tavares, *Journal of Chromatography* A, **2002**, 979, 409-416.

22. L. M. Cardenas, D. J. Brassington, B. J. Allan, H. Coe, B. Alicke, U. Platt, K. M. Wilson, J. M .C. Plane, S. A. Penkett, *Journal of Atmospheric Chemistry,* **2000**, 37, 53-80.

23. A. Fried, B. P. Wert, B. Henry, J. R. Drummond, *Spectrochimica Acta* A, **1999**, 55, 2097-2110.

24. J. P. Lodge, J. B. Pate, *Science*, **1996**, 153, 408 ; R. J. Breeding, J. P. Lodge, J. B. Pate, D. C. Sheesley, H. B. Klonis, B. Fogel, J. A. Anderson, T. R. Englert, P. L. Haagenson, R. B. McBeth, A. L. Morris, R. Pogue, A. F. Wartburg, *J. Geophys. Res*, **1973**, 78, 7057.

25. W. Klippel, P. Warneck, *Geophys. Res. Lett*, **1978**, 5, 177.

26. P. Carlier, H. Hannachi, G. Mouvier, *Atmospheric Environment*, **1986**, 20, 2079.

27. B. J. Finlayson-Pitts, J. N. Pitts, Chemistry of the Upper and Lower Atmosphere, **1999**, 592-593.

28. www.epa.gov/iaq/formalde.html.

29. T. Godish, Indoor Air Pollution Control, Lewis Publishers, Boca Raton, FL, 2nd edn, **1989**, 37.

30. D. J. Moschandreas and S. M. Gordon, Organic Chemistry of the Atmosphere, CRC Press, Boca Raton, FL, 1st edn, **1991**, 130.

31. S. M. Hays, R. V. Gobbell, and N. R. Gauick, Indoor Air Quality: Solution and Strategies, McGraw Hill, New York, **1995**, 55.

32. Y. Yokouchi, H. Mukai, K. Nakajima, Y. Ambe, *Atmos. Environ*, **1990**, 24, 439.

33. R. Jeltes, Th. R. Thijsse, *Atmos. Environ,* **1978,** 12, 556.

34. S. P. Levine, T. M. Harvey, T. J. Waeghe, R. H. Shapiro, *Anal. Chem*, **1981**, 53, 805.

35. S. J. Swarin, F. Lipari, *J. Liq. Chromatography*, **1983**, 32, 33.

36. A. L. Lazrus, K. L. Fong, A. J. Lind, *Anal. Chem*, **1988**, 60, 1074.

37. S. Yamagishi, M. Tsuchiya, Comodia, *Atmos. Environ*, **1994**, 74, 511.

38. J. E. Harrington, K. C. Smyth, *Chem. Phys. Lett*, **1993**, 202, 196.

39. D. J. Shin, T. Dreier, J. Wolfrum, *Appl. Phys*. B, **2001**, 72, 257.

40. P. H. Paul, H. N. Najim, in: Proceedings of the 27 th Symposium (Int) on Comb./Comb. Inst, **1998**, 43.

41. R. Bombach, B. Kappeli, *Appl. Phys*. B, **1999**, 68, 251.

42. B. Bauerle, F. Hoffmann, F. Behrendt, J. Warnatz, in: Proceedings of the 25 th Symposium (Int) on Comb./Comb. Inst, **1994**, 135.

43. S. Bockle, J. Kazenewadel, T. Kunzelmann, D. I. Shin, C. Schulz, *Applied Physics* B, **2003**, 70, 733.

44. A. Burkert, W. Triebel, H. Stafast, J. Konig, in: Proceedings of the 29 th Symposium (Int) on Comb./Comb. Inst, **2002**, 2645.

45. R. J. H. Klein-Douwel, J. B. Jeffries, J. Luque, G. P. Smith, D. R. Crosley, *Combust. Sci. Technol,* **2001**, 167, 291.

46. E. J. Woodbury, W. K. Ng, *Proc. IRE*, **1962**, 50, 2347.

47. G. Eckhardt, R. W. Hellwarth, F. J. McClung, S. E. Schwarz, D. Weiner, E. J. Woodbury, *Phys. Rev. Lett*., **1962**, 9, 455.

48. J. D. Rodgers, *J. Chem. Phys*, **1990**, 94, 4011-4015.